IP_{3-4} kinase Arg1 regulates cell wall homeostasis and surface architecture to promote clearance of *Cryptococcus neoformans* infection in a mouse model

Cecilia Li[1,2,3*], Sophie Lev[1,2,3*], Desmarini Desmarini[1], Keren Kaufman-Francis[1,3], Adolfo Saiardi[4], Ana P.G. Silva[5], Joel P. Mackay[5], Philip E. Thompson[6], Tania C. Sorrell[1,2,3,7] and Julianne T. Djordjevic[1,2,3,7#]

[#]Corresponding author: julianne.djordjevic@sydney.edu.au

*CL and SL contributed equally to this work

[1]Centre for Infectious Diseases and Microbiology, The Westmead Institute for Medical Research, 176 Hawkesbury road, Westmead NSW 2145, Australia; [2]Sydney Medical School-Westmead, The University of Sydney, Westmead NSW 2145, Australia; [3]Marie Bashir Institute for Infectious Diseases and Biosecurity, University of Sydney, NSW Australia; [4]Medical Research Council Laboratory for Molecular Cell Biology, University College London, Gower street, London WC1E 6BT, UK; [5]School of Life and Environmental Sciences, The University of Sydney, Camperdown, NSW 2006, Australia; [6]Medicinal Chemistry, Faculty of Pharmacy and Pharmaceutical Sciences, Monash University, 381 Royal Parade, Parkville , VIC 3052, Australia; [7]Westmead Hospital, Westmead, NSW 2145, Australia.

Keywords: *Cryptococcus neoformans*; inositol pyrophosphate; PP-IP_5; IP_7; inositol polyphosphate kinase; virulence; molecular fungal pathogenesis; mouse model; meningitis; cell wall.

Abstract

We previously identified a series of inositol polyphosphate kinases (IPKs), Arg1, Ipk1, Kcs1 and Asp1, in the opportunistic fungal pathogen *Cryptococcus neoformans*. Using gene deletion analysis, we characterized Arg1, Ipk1 and Kcs1 and showed that they act sequentially to convert IP_3 to PP-IP_5 (IP_7), a key metabolite promoting stress tolerance, metabolic adaptation and fungal dissemination to the brain. We have now directly characterized the enzymatic activity of Arg1, demonstrating that it is a dual specificity (IP_3/IP_4) kinase producing IP_5. We showed previously that IP_5 is further phosphorylated by Ipk1 to produce IP_6, which is a substrate for the synthesis of PP-IP_5 by Kcs1. Phenotypic comparison of the *arg1*Δ and *kcs1*Δ deletion mutants (both PP-IP_5-deficient) reveals that *arg1*Δ has the most deleterious phenotype: while PP-IP_5 is essential for metabolic and stress adaptation in both mutant strains, PP-IP_5 is dispensable for virulence-associated functions such as capsule production, cell wall organization, and normal *N*-linked mannosylation of the virulence factor, phospholipase B1, as these phenotypes were defective only in *arg1*Δ. The more deleterious *arg1*Δ phenotype correlated with a higher rate of *arg1*Δ phagocytosis by human peripheral blood monocytes and rapid *arg1*Δ clearance from lung in a mouse model. This observation is in contrast to *kcs1*Δ, which we previously reported establishes a chronic, confined lung infection. In summary, we show that Arg1 is the most crucial IPK for cryptococcal virulence, conveying PP-IP_5–dependent and novel PP-IP_5–independent functions.

Introduction

Cryptococcus neoformans is a major opportunistic fungal pathogen in immunocompromised individuals, especially those with HIV/AIDS (reviewed in [1, 2, 3]).

Although the primary site of infection is the lung, immunosuppressed patients typically present with meningoencephalitis, which is fatal without treatment [1, 2, 3]. Even with appropriate treatment, (amphotericin B and 5 flucytosine, followed by long-term fluconazole), unacceptably high mortalities are reported [1, 2, 3], highlighting the need to develop more effective antifungal therapies. Current drugs target the ergosterol biosynthetic pathway/cell membrane (azoles, amphotericin B), RNA (5 flucytosine) or the cell wall biosynthetic enzyme, glucan 3 synthase (echinocandins). Amphotericin B exhibits significant haematological and nephrological toxicity [4], while echinocandins are ineffective against the *Cryptococcus* complex [5 6]. Furthermore, fluconazole-resistant *C. neoformans* has been reported in Sub-Saharan Africa and South East Asia [7 8]. A detailed understanding of the biology of *C. neoformans* and other pathogenic fungi is essential for the identification of new drug targets.

The ability of *C. neoformans* to adapt to the host environment is mediated by several key signalling pathways (reviewed in [9]). These pathways also fine-tune secretory mechanisms to facilitate export of virulence factors and cell wall remodelling enzymes [10 11 12]. Secreted virulence factors include the cell-wall associated enzyme, laccase (produces melanin) [13], the cell wall-associated and secreted invasin, phospholipase B1 (Plb1) [14], and polysaccharide capsule building blocks[15, 16] which attach to the cell wall [17, 18]. Secretion is therefore essential for regulating fungal virulence and surface architecture, the latter of which impacts recognition by the innate immune system [19].

Using a combination of gene deletion analysis, inositol polyphosphate (IP) and phenotype profiling and enzyme activity assays, we identified and characterised the phospholipase C1/inositol polyphosphate kinase (Plc1/IPK) pathway, and showed that it is essential for the production of several virulence traits and for regulating cell wall integrity. Specifically, we showed that Plc1, the homologue of the PLC1δ isoform in mammalian cells, hydrolyzes the membrane phospholipid, phosphatidylinositol 4,5-bisphosphate (PIP_2) to generate inositol 1,4,5-trisphosphate (IP_3) [20]. Several IPK enzymes, i.e. Arg1, Ipk1, Kcs1 and Asp1, then act sequentially to generate a series of IPs and inositol pyrophosphates (PP-IPs).

IPs and PP-IPs are present in all eukaryotes and play critical roles in cellular function (reviewed in [21, 22]). Several lines of evidence support fungal IPKs as being candidate targets for antifungal drug development. Firstly, the IPK pathway is non-linear and more complex in mammalian cells than it is in fungi, and generates a wider variety of IP species. Secondly, some mammalian enzymes exhibit functional redundancy, e.g. inositol polyphosphate multikinase (IPMK) and IP3K both convert IP_3 to IP_4. In contrast, each IP conversion step in *C. neoformans* is catalyzed by a single IPK. Thirdly, IPKs share a low sequence homology with their mammalian counterparts (e.g. human IPMK and *C. neoformans* Arg1 are only 19% identical). Finally, a homology search reveals that IPKs are also non-redundant in other fungal pathogens, for example *Candida albicans*, suggesting that IPKs are a possible target for panfungal therapy.

The first IP produced by the Plc1/IPK pathway is IP_3, which we showed serves as a substrate for Arg1 [20]. In comparison with WT, IP_3 accumulated in the *ARG1* deletion mutant (*arg1*Δ), whereas all IP and PP-IP species downstream of IP_3 were depleted, confirming, indirectly, that Arg1 is an IP_3 kinase [23]. We also identified a homolog of Arg1 in the cryptococcal genome, Arg2, but found that it neither played a role in IP_3 conversion nor in virulence [20]. Ipk1, Kcs1, and Asp1 were later identified as IP_5, IP_6 and PP-IP_5 kinases, respectively, acting downstream of Arg1 [23, 24].

Phenotypic characterization of the *arg1*Δ mutant demonstrated that Arg1 is essential for thermotolerance, cell wall integrity and vacuolar homeostasis [20]. The *arg1*Δ mutant was also hypovirulent in a *Galleria melonella* infection model [20]. In contrast, the terminal IPK, Asp1, and its product, $(PP)_2$-IP_4, were dispensable for cellular function and virulence [23]. Using the *kcs1*Δ mutant, which is deficient in PP-IP_5 and $(PP)_2$-IP_4, we showed that PP-IP_5 is crucial for cell wall integrity, response to stress, metabolic adaptation to the utilization of diverse carbon sources and dissemination of infection in a mouse inhalation model [20, 23, 24]. Although the *ipk1*Δ deletion mutant is also deficient in PP-IP_5 and IP_6, attenuation of its phenotypes was not as severe as in the *kcs1*Δ mutant due to the accumulation of PP-IP_4, which we concluded partially compensates for the absence of PP-IP_5 [24]. Similar to *kcs1*Δ, the *arg1*Δ mutant does not produce PP-IP_5, suggesting that the absence of PP-IP_5 is responsible, at least in part, for the phenotypic defects of *arg1*Δ.

In this study we demonstrate that recombinant Arg1 is a dual specificity kinase, converting IP_3 to IP_4 and IP_4 to IP_5. We also perform extensive phenotypic comparison of the *arg1*Δ and *kcs1*Δ mutants, and identify Arg1 functions that are independent of PP-IP_5. These functions include capsule production, *N*-linked mannosylation and secretion of the virulence determinant Plb1 and cell wall organization. We show that via these functions, Arg1 affects recognition of *C. neoformans* by the host immune system and its ability to establish a lung infection.

Results

Cryptococcal Arg1 restores defective phenotypes in the *S. cerevisiae arg82*Δ mutant.

To assess the degree of functional similarity between Arg1 and its orthologue in *S. cerevisiae*, Arg82, we tested whether *ARG1* could restore the growth defects observed in the *S. cerevisiae arg82*Δ mutant in a complementation assay. Arg82 acts as both an IP_3 and an IP_4 kinase to produce IP_5. Both the *arg1*Δ mutant and the *arg82*Δ mutant exhibit a pleiotropic phenotype [25, 26]. Phenotypes that are shared by *arg1*Δ and *arg82*Δ include defective mating and high temperature sensitivity [20]. The *arg82*Δ mutant is also auxotrophic for arginine and ornithine [25-27]. In Figure 1, we show that the introduction of cryptococcal *ARG1* into the *S. cerevisiae arg82*Δ mutant restored its growth at elevated temperature and on ornithine as a sole nitrogen source. Furthermore, *ARG1* restored

*arg82*Δ tolerance to SDS and the cell wall perturbing agent calcofluor white (CFW). These findings support the role of Arg1 as an IP_3 and an IP_4 kinase, similar to Arg82.

Arg1 and Arg82 contribute differentially to stress adaptation of *C. neoformans* and *S. cerevisiae,* respectively.

To compare the contribution of Arg1 and Arg82 to stress tolerance in *C. neoformans* and *S. cerevisiae,* respectively, the deletion mutants were exposed to elevated temperature and ionic stress. Figure 2 demonstrates that cryptococcal Arg1 and Kcs1 contribute more significantly to temperature tolerance in *C. neoformans* than Arg82 and Kcs1 do in *S. cerevisiae*. However, in contrast to Arg82 and Kcs1 in *S. cerevisiae,* cryptococcal Arg1 and Kcs1 contribute very little to adaptation to ionic stress in *C. neoformans.*

Recombinant Arg1 has IP_3 and IP_4 kinase activities

In our previous study, we used HPLC-based IP profiling of WT and *arg1*Δ to demonstrate indirectly that Arg1 is an IP_3 kinase: the *arg1*Δ mutant accumulated IP_3, while IP_{4-6}, PP-IP_5 and $(PP)_2$-IP_4 were absent [23]. To obtain direct evidence that, similar to Arg82, Arg1 has both IP_3 and IP_4 kinase activities, we produced recombinant His-tagged Arg1 in *E. coli* (Figure 3A). We found that overnight induction of His-Arg1 expression at 22°C resulted in the highest yield of soluble, full-length fusion protein. The enzyme was then purified in two steps using cobalt affinity and anion exchange chromatography.

To establish IP_5 as the end-product of Arg1 catalysis, purified enzyme (final concentration 5 ng/µl) was incubated with IP_3 and ATP for 20 min and 2 hours. Phosphorylation products were analyzed by polyacrylamide gel electrophoresis followed by Toluidine Blue staining. The results in Figure 3B demonstrate the complete conversion of IP_3 to IP_5 by Arg1 in 20 minutes. A faint band migrating at a rate similar to that of IP_6 was observed in both Arg1 reactions. This band is most likely PP-IP_4, which is also a product of purified IPMK [28]. To confirm IP_4 as the intermediate product in Arg1-mediated IP_5 production, purified Arg1 at different concentrations (1-10 ng/µl) was incubated with IP_3 and ATP for 10 minutes. The results in Figure 3B demonstrate direct correlation between the amount of Arg1 and the amount of IP_4 and IP_5 produced, establishing Arg1 as a dual specificity (IP_3 and IP_4) kinase.

To determine the kinetic properties of Arg1, we used a bioluminescent assay to quantify Arg1-mediated ATP consumption (Figure 3C). The K_m of Arg1 for ATP was estimated to be 184 µM and the V_{max} 2.35 µM/min.

Sensitivity of cryptococcal *arg1*Δ and *kcs1*Δ to nutrient and cell wall stress highlights the importance of PP-IP_5 for stress adaptation

We previously described the defective phenotype of the *arg1*Δ mutant [20]. To distinguish PP-IP_5-dependent and -independent defects, we performed a comprehensive phenotypic comparison of the *arg1*Δ and *kcs1*Δ mutants using drop dilution assays (Figure 4). The results demonstrate that both mutants are hypersusceptible to multiple

stress conditions including alkaline pH, cell wall perturbing agents and ER stress (tunicamycin and DTT). Growth of both mutants was also slower on blood agar, on carbon sources other than glucose, in an environment deficient in free phosphate and at high temperature (37°C). At 37°C, *arg1*Δ growth was more severely compromised than *kcs1*Δ growth, while under cell culture conditions (37°C/5% CO_2, pH 7.4), growth of *kcs1*Δ and *arg1*Δ was equally compromised. This was likely due to the basic pH, to which both mutants are equally sensitive (Figure 4). Taken together, these results confirm the importance of PP-IP_5 in stress adaptation.

_arg1_Δ and _kcs1_Δ mutants differ in cell wall organisation, vacuolar morphology and capsule production

Cell wall organization: The hypersusceptibility of the *arg1*Δ and *kcs1*Δ mutants to cell wall perturbing agents prompted us to visualize cell wall ultrastructure using transmission electron microscopy (TEM). In comparison to WT and the *kcs1*Δ mutant, *arg1*Δ cells were often enlarged. The cell walls of the enlarged cells were disorganized and multi-layered (Figure 5). In WT, the cell wall thickness ranged between 100 and 150 nm, while in the enlarged *arg1*Δ cells it often reached 300-500 nm. Unexpectedly, given that the hypersusceptibility of the *kcs1*Δ mutant to cell wall perturbing agents is greater than or equal to that of the *arg1*Δ mutant, the cell walls of this mutant were similar to those of the WT in thickness and morphology (Figure 4).

Vacuolar morphology: Using differential interference contrast and fluorescence microscopy we previously demonstrated that a significant proportion of *arg1*Δ cells were

larger than those of WT, and that *arg1*Δ cells had enlarged vacuoles, which were likely to have formed by fusion of smaller vacuoles [20]. We therefore used the lipophilic dye, FM 4-64, to label the endocytic pathway in WT, *arg1*Δ and *kcs1*Δ as described in [20]. We found that in contrast to *arg1*Δ, *kcs1*Δ cells rarely produced enlarged vacuoles and their cell size was similar to that of WT (Figure 6). Images obtained by TEM (Figure 5) similarly show enlarged vacuoles in *arg1*Δ cells, as reported previously [20].

Capsule production: Capsules were induced following growth in minimal medium, and visualized under the light microscope following negative staining with India Ink (Figure 7). Statistical analysis of capsule size showed that *arg1Δ* capsules are smaller than those of WT and *kcs1Δ*, and that *kcs1Δ* capsules are larger than those of WT and *arg1Δ*. We also note that vacuoles are significantly larger in *arg1Δ* than in WT and *kcs1Δ*, supporting the FM 4-64 data in Figure 6.

Phospholipase B1 secretion is blocked in *arg1*Δ

To further investigate the differences in cell wall architecture between *arg1*Δ and *kcs1*Δ, we focused on the secretory pathway, which is essential for the export of mannoproteins involved in cell wall integrity. One of these mannoproteins is the virulence factor Plb1 [29, 30]. Not only is Plb1 a fungal 'invasin' with a role in cell wall integrity [14], it is also a marker of the classical secretion pathway in *C. neoformans* [31, 32]. Plb1 acquires a glycosylphosphatidylinositol (GPI) anchor in the ER/Golgi to enable Plb1 attachment to the cell surface [14, 33]. However, Plb1 can also become detached from the cell surface and released to the external milieu [14, 34].

The levels of secreted and cell-associated Plb1 in WT, *arg1*Δ and *kcs1*Δ were assessed by Western blotting with the anti-Plb1 antibody. Figure 8A demonstrates that the majority of Plb1 in WT samples is released extracellularly. Conversely, the *arg1*Δ mutant secreted very little Plb1 but produced more cell-associated Plb1 than WT, indicative of a Plb1 secretion block. In contrast, no Plb1 was detected in the secretions and very little Plb1 was produced intracellularly in *kcs1*Δ, despite the *PLB1* mRNA level being similar to that of the WT (Fig. 8B).

Plb1 is hyper *N*-linked mannosylated in *arg1*Δ but not in *kcs1*Δ

In Figure 8A, we observed that Plb1 produced by *arg1*Δ has a higher apparent molecular weight on SDS-PAGE (170 kDa) than WT (120 kDa). We showed previously that approximately 30% of the molecular weight of Plb1 is attributable to *N*-linked mannosylation [35], and that preventing the acquisition of *N*-linked mannosylation by site-directed mutagenesis prevents Plb1 transport to the cell surface in a heterologous expression system [30]. To determine whether the increase in Plb1 size in the *arg1*Δ mutant (Figure 8A) is due to abnormal processing of *N*-linked mannose sugars in the Golgi, we treated the secretions collected from WT and *arg1*Δ with *N*-glycosidase F (PNGase F) and assessed protein size by anti-Plb1 Western blotting (Figure 9A). Secretions were chosen over cell-associated fractions as TRIzol-extracted cellular proteins are less amenable to enzymatic treatment due to the need to solubilize them in a strong detergent. Although *arg1*Δ secretes less Plb1 than WT, sufficient Plb1 protein

was present in *arg1*Δ secretions to observe a shift in molecular weight following PNGase F treatment. As shown in Figure 9A, PNGase F treatment reduced the size of Plb1 in both WT and *arg1*Δ to approximately 65 kDa, consistent with the molecular weight of Plb1 as deduced from its amino acid sequence. These results confirm that Plb1 is hyper *N*-mannosylated in the *arg1*Δ mutant.

To determine whether hyper *N*-linked mannosylation in the *arg1*Δ mutant extends to all secreted proteins, PNGase F treated and untreated secretions were resolved by SDS-PAGE. The gels were then stained consecutively with a glycoprotein-specific stain (Figure 9B) and Coomassie Blue (Figure 9C). Differences were observed in the glycoprotein profile of the secretomes from untreated WT and *arg1*Δ (Figure 9B). PNGase F-treated WT and *arg1*Δ secretomes had a fainter stain than the corresponding untreated sample, indicating that most of the proteins in each secretome are *N*-linked mannosylated. However, in contrast to Plb1 in Figure 9A, Coomassie staining unexpectedly demonstrated differences in the profiles of PNGase F-treated WT and *arg1*Δ secretions, indicating that the composition of the *arg1*Δ secretome is altered; this prevented assessment of whether *N*-linked mannosylation, in general, is also affected. Interestingly, we observed a highly abundant protein with a MW of 25 kDa in WT, but not *arg1*Δ. This protein appeared to be glycosylated as it stained strongly with the glycoprotein stain, but its MW was unchanged following PNGase F treatment, consistent with the presence of *O*-linked sugars.

Arg1 is essential for lung colonization and dissemination in a murine inhalation model.

To assess the impact of *ARG1* deletion on cryptococcal virulence, we compared the survival of mice infected with WT, *arg1*Δ and *arg1*Δ + *ARG1* using the inhalation model, which mimics the natural route of infection in humans (Figure 10). All *arg1*Δ-infected mice were healthy and had lost no weight by 60-days post-infection. In comparison, all WT and *arg1*Δ + *ARG1*-infected mice succumbed to infection by day 21. The median survival time of the WT and *arg1*Δ + *ARG1*-infected mice was 15 and 16.5 days, respectively. The difference in survival of *arg1*Δ-infected mice versus WT- and *arg1*Δ + *ARG1*-infected mice was statistically significant (Figure 10A).

Fungal burdens in the lung and brain of WT and *arg1*Δ–infected mice were also assessed. In contrast to *kcs1*Δ, which was avirulent, but established a chronic, localized, asymptomatic lung infection that persisted for 50-days post-inoculation [23], *arg1*Δ infection was cleared from mouse lung between 3 and 7-days post-inoculation (Figure 10B). Consistent with the absence of established lung infection, no *arg1*Δ CFUs were detected in the brain by day 14, which is the time when WT brain burdens were the highest (Figure 10B). Brain tissue harvested from *arg1*Δ-infected mice upon termination of the study at day 60 revealed no evidence of cryptococcal dissemination to the CNS (data not shown). Histological analysis showed that by 3-days post-inoculation, WT cryptococci had colonized the lung parenchyma (Figure 10C). In contrast, only a few small acapsular cryptococci are observed in the lung parenchyma

of *arg1*Δ-infected lungs at this time point, with lung pathology appearing otherwise healthy.

We also assessed the survival and organ burdens of mice infected with WT and *arg1*Δ in a model of disseminated cryptococcosis where mice were infected via the retro-orbital plexus as previously described [36]. In this model, WT-infected mice all succumbed to infection by day 10 as previously reported [36]. However, following *arg1*Δ infection, mice remained asymptomatic over a 40-day infection period and there was no evidence of infection in blood, spleen, lungs or brain (data not shown).

Phagocytosis of *arg1*Δ is greater than that of *kcs1*Δ

Studies in mouse infection models have demonstrated that monocytes are the first line of defence against *C. neoformans*, either containing or clearing the infection [37, 38]. Given that the *arg1*Δ mutant has an altered surface (Figures 5, 7 and 9), we compared the phagocytosis of WT, *arg1*Δ and *kcs1*Δ by human peripheral blood monocytes (PBMCs) using flow cytometry. Figure 11 demonstrates that the extent of phagocytosis of *arg1*Δ was 7 and 2.5 times greater than that of *kcs1*Δ and WT, respectively.

The PP-IP_5-dependent functions of Arg1 involved in stress adaptation, and its novel PP-IP_5-independent functions relating to cell wall homeostasis, cell surface architecture and host recognition, are summarized in Figure 12. The combination of these functions contributes to the essential role of Arg1 in establishment of lung infection.

Discussion

Arg1 is a dual-specificity IP_3/IP_4 kinase

Complementation studies demonstrated functional similarities between Arg1 and the IP_{3-4} kinase in *S. cerevisiae* (Arg82), as expression of Arg1 in the *arg82*Δ mutant restored Arg82-dependent phenotypes. We also showed directly that recombinant Arg1 is a dual specificity kinase that rapidly converts IP_3 to IP_5 (via IP_4) in the presence of ATP. Characterization of the enzymatic properties of Arg1 determined a K_m of 184 μM for ATP as compared to 74 μM and 17 μM for chicken GgIP3K-A and human IPMK, respectively [39]. These values are all significantly lower than the estimated intracellular concentration of ATP (~1 mM), suggesting that these IP_3 kinases are continuously occupied by ATP. In contrast to IP_3 kinases, the K_m of Kcs1 enzymes for ATP is in the millimolar range [40, 41]. The lower affinity of Kcs1 for ATP is therefore consistent with the biosynthesis of PP-IP_5, but not IP_5, being linked to the availability of cellular ATP and hence PP-IP_5 acting as a sensor of cellular energy status [21].

Similarity of the *arg1*Δ and *kcs1*Δ stress sensitivity phenotypes confirms the importance of PP-IP_5 for stress adaptation

Using the *kcs1*Δ mutant, we showed that PP-IP_5 is essential for stress tolerance, metabolic adaptation and dissemination of infection in a mouse inhalation model [23]. Our previous studies also showed that the *arg1*Δ mutant, which is deficient in all IPs

downstream of IP_3, was defective in many cellular functions and virulence-related phenotypes [20]. However, direct comprehensive comparison of *arg1*Δ and *kcs1*Δ phenotypes to assess the PP-IP_5-dependent and -independent contribution of Arg1 to cellular function had not been undertaken. We therefore performed extensive phenotypic analysis of *arg1*Δ and *kcs1*Δ and demonstrated that the phenotypes of both mutants overlap significantly. This included hypersusceptibility to cell wall perturbing and other stress-inducing agents. Furthermore, the ability of *arg1*Δ and *kcs1*Δ to metabolize alternative carbon sources was diminished. This was supported by our published RNAseq data[23]. This data demonstrated that the expression of genes encoding mitochondrial enzymes essential for the utilization of alternative carbon source is down-regulated in *arg1Δ* and *kcs1Δ*, while the expression of glycolytic enzymes is increased. Given that PP-IP_5 is absent in *arg1*Δ and *kcs1*Δ, the results demonstrate the importance of PP-IP_5 for adaptation to diverse stress conditions, potentially via pyrophosphorylation of key regulatory proteins. In support of this, the presence of inositol pyrophosphates leads to a decrease in the glycolytic/mitochondrial metabolic ratio in *S. cerevisiae.* This effect is attributable, at least in part, to pyrophosphorylation of the major glycolytic transcription factor Gcr1: pyrophosphorylated Gcr1 binds Gcr2 with lower affinity, leading to reduced transcription of genes encoding glycolytic enzymes [42].

Figure 4 demonstrates that PP-IP_5 is required for growth under physiological conditions (RPMI media, pH7.4 5%CO_2/37^{o}C). Despite this, the *kcs1*Δ mutant persisted in the

lungs of infected mice[23], while *arg1*Δ was cleared (Figure 10). This result suggests that PP-IP_5-independent factors contribute to *arg1*Δ clearance from lung *in vivo*.

Arg1 regulates capsule production, *N*-linked mannosylation, secretion and cell wall morphology independently of PP-IP_5

We identified several phenotypes that were specifically defective in *arg1*Δ, but not *kcs1*Δ, and which must therefore result from factors other than the absence of PP-IP_5. These phenotypes include diminished capsule production, hyper *N*-linked mannosylation of Plb1, that was associated with failure of its release from the cell, an altered general secretion profile, and cell walls with abnormal morphology. *Arg1*Δ was also more rapidly phagocytozed by monocytes than *kcs1*Δ. Given that cell wall integrity is dependent on secretory functions, such as correct mannosylation and secretion, an alteration in these functions in *arg1*Δ potentially contributes to altered cell wall morphology and to smaller capsules, since capsule is associated with the cell wall [17, 18]. This in turn could affect recognition by the immune system. *arg1*Δ-specific phenotypes coincided with avirulence of the *arg1*Δ mutant in a mouse model and rapid clearance of *arg1*Δ from the lungs (Figure 10). This is in contrast to *kcs1*Δ, which had normal cell wall morphology and established a subclinical infection that was confined to the lung [23]. It is possible that the *arg1*Δ mutant is rapidly cleared from the lung because it is more rapidly phagocytozed by cells of the innate immune system. Reduced capsule size in the *arg1*Δ mutant is likely to expose more surface β-glucan and mannoprotein to the

binding of opsonising antibody, thereby increasing phagocyte recognition and phagocytosis, as has previously been reported for acapsular mutants [43].

Interestingly, less apparent alteration in cell wall organization was detected in *kcs1Δ* by TEM analysis as compared to *arg1Δ*. This was despite *kcs1Δ* displaying a more severe growth defect in the presence of cell wall perturbing reagents. Compensatory changes, such as alteration of cell wall architecture, may therefore be essential for maintaining the viability of *arg1Δ*. As the absence of Kcs1 is less detrimental, resulting in loss of only PP-IP_5-dependent functions, the compensatory changes are less apparent, or not required, in *kcs1Δ*. Compensatory changes in the cell wall have been reported in other fungi where cell wall stress caused by mutations or antifungal drugs, triggered increased deposition of chitin in the cell wall [44], [45], [46].

In contrast to *arg1Δ*, Plb1 protein was barely detectable in *kcs1Δ* despite the *PLB1* mRNA level being similar to that of the WT (Fig. 8). Why Plb1 protein production is reduced in *kcs1*Δ, but not in *arg1Δ* is unknown but is most likely due to a defect in translation of the *PLB1* mRNA. In our previous publication[23], we demonstrated that exposure of mannoproteins on the surface of the *kcs1*Δ mutant, as detected by concanavalin A binding, was reduced, and that this coincided with the reduced expression of a subset of mannoprotein-encoding genes. RNAseq analysis also shows that expression of these mannoproteins, but not Plb1, is reduced in the *arg1*Δ mutant (GEO accession GSE78824). We propose that expression of other mannoproteins, including Plb1, could be upregulated in the *arg1*Δ mutant (but not in the *kcs1Δ* mutant)

in an attempt to compensate for a defective cell wall, with Plb1 being more highly associated with the cell periphery.

We propose that excess IP_3 and/or the absence of IP_4/IP_5 are likely to contribute to the PP-IP_5-independent phenotypes observed in *arg1*Δ. An excess of IP_3 might be detrimental by competing with phosphoinositides and IPs for binding to the pleckstrin homology (PH) domain, and/or other specialized protein domains, thus interfering with the regulation of their functions [47, 48]. Alternatively, an excess of IP_3 could potentially inhibit Plc1 activity via feedback inhibition, since IP_3 is a product of Plc1-mediated PIP_2 hydrolysis [20]. In support of this, the *PLC1* deletion mutant (*plc1Δ*) and the *arg1Δ* mutant have a similar phenotype, including cell walls with abnormal morphology, blocked release of Plb1 from the cell periphery and rapid pulmonary clearance in a mouse model [34], which are all PP-IP_5 independent. The absence of IP_4 could affect gene expression since IP_4 is required for the incorporation of the histone deacetylase HDAC3 into a repressive complex, and for its enzymatic activity in mammalian cells [49, 50]. Both IP_4 and IP_5 have been reported to bind to PH domains [49, 50, 51, 52]. Hence the absence of IP_4/IP_5 in the *arg1Δ* mutant could affect the function of proteins containing PH domains.

In summary, the combination of PP-IP_5 -dependent and -independent functions render Arg1 the most important IPK for the virulence of *C. neoformans* in animal models. Its PP-IP_5-independent roles in regulating cryptococcal surface topology likely affect recognition by the host immune system, resulting in clearance in mouse models. The

key role of Arg1 in virulence, coupled with its low sequence similarity and non-redundant function as compared to mammalian cells, make Arg1 a candidate target for antifungal drug development.

Material and methods

Fungal strains and media

Cryptococcal strains used in this study were wild-type (WT) *C. neoformans* var. *grubii* strain H99 (serotype A, MAT*α*) and the isogenic strains, *arg1*Δ, *kcs1*Δ and reconstituted *arg1*Δ (*arg1*Δ + *ARG1*), which were created as previously described in [20, 23]. Strains were routinely grown on YPD (1% yeast extract, 2% peptone and 2% dextrose) or Sabouraud (SAB) agar (1% peptone, 4% glucose, 1.5-2% agar). The *S. cerevisiae* deletion mutants, *arg82*Δ *(*#4003531) and *kcs1*Δ (#4003956), which were derived from the parental strain BY4741, were obtained from the ATCC.

Expression, purification and enzymatic characterisation of recombinant Arg1

Arg1 cDNA was amplified using primers ARG1-BglII -s (tacgagatctGACCTGCCCCTCACCCTCG) and ARG-EcoRI-a (CAAGGAATTCTCAAACACAACCCCGTTCAACC) and cloned into the pRSET expression vector to allow production of a 6 histidine-tagged Arg1 fusion protein in Rosetta™ (DE3) *E. coli* strain. Cultures were incubated overnight at 37°C, diluted 1:100 and incubated at 37°C until the OD_{600} reached 0.6-0.8. 1 mM IPTG was then added to

induce expression of His-tagged Arg1 and the cultures were incubated overnight at ambient temperature. The cells were washed with water, resuspended in lysis buffer (500 mM NaCl; 25 mM Tris–HCl pH 8.0), sonicated and centrifuged to remove debris.

His-Arg1 fusion protein in the supernatant then underwent two rounds of purification. The first round involved using a His GraviTrap TALON affinity column (GE Healthcare, Cat. No. 29-0005-94). The column loaded with His-Arg1 was washed with 10 mL of wash buffer I (600 mM NaCl; 0.1% (v/v) Trition X-100; 25 mM Tris–HCl pH 8.0), and then with 10 mL of wash buffer II (100 mM NaCl; 0.1% (v/v) Trition X-100; 25 mM Tris–HCl pH 7.4). His-Arg1 was eluted from the column with the elution buffer (100 mM NaCl, 200 mM imidazole, 25 mM Tris pH 7.5). His-Arg1 protein was then diluted 3.5-fold in a buffer containing 20 mM Tris pH 7.4, 1 mM DTT and 1 mM $MgSO_4$ and concentrated using an Amicon concentrator (10 kDa cutoff). The second round of purification involved using an anion exchange column; His-Arg1 was eluted from this column using a NaCl gradient (buffer A: 30 mM NaCl, 20 mM Tris pH 7.4, 1 mM $MgSO_4$, 1 mM DTT; buffer B: similar to A, but with NaCl 1000 mM). The purified His-Arg protein was then diluted in a storage buffer (100 mM NaCl; 1 mM $MgSO_4$; 1 mM DTT; 0.05% (v/v) CHAPS; 20 mM Tris–HCl pH 7.4, 40% glycerol) at 500 µg/mL, snap-frozen and stored in aliquots at -80°C.

Routinely, Arg1 activity assay (10 µL) contained 5 µL 2X reaction buffer (40 mM Hepes pH 6.8; 200 mM NaCl; 12 mM MgCl; 2 mM DTT), 200 µM IP_3, 500 µM ATP and 20 ng

purified Arg1. The reactions were incubated at ambient temperature for up to 30 min, and ATP consumption was measured using a bioluminescent ATP assay kit (Kinase-Glo® Max Luminescent Kinase Assay Kit, Promega). To determine the kinetic properties of Arg1, the reactions were performed using starting ATP concentrations ranging between 50-500 μM ATP, and the ATP concentration was assessed after 0, 10, 20 and 30 min. The assay was performed twice, each in triplicate. K_m and V_{max} were determined using the Michaelis-Menten model.

To establish that Arg1 is an IP_{3-4} kinase using PAGE, 40 μl reactions were set up as described above, using different final concentrations of Arg1 (1 to 10 ng/μl). The reactions were terminated after 10 min, 20 min or 2 hours, as indicated in Figure 3, by the addition of EDTA (10 mM). Visualization of IPs (Arg1 substrates/products) using PAGE and Toluidine Blue staining was performed as described in [53].

Yeast complementation assay

ARG1 cDNA from *C. neoformans* was amplified using the forward primer ccaactagtATGGACCTGCCCCTCACCCT and reverse primer cgcttaattaaTCAAACACAACCCCGTTCAAC, and cloned into the pESC-LEU expression vector. The vectors were used to transform strain BY4741 (*S. cerevisiae*) and the *arg1*Δ mutant using a Frozen-EZ Yeast Transformation II Kit (Zymo Research). Complemented and control strains were tested by growing on standard SD medium without leucine at high temperature (39°C) or in the presence of 0.1 mg/mL Calcofluor

white (CFW) or 0.0075% SDS. To test growth on different nitrogen sources, SD was prepared without amino acids and ammonium sulfate, and supplemented with ornithine or ammonium sulfate as the sole nitrogen source. Stress tolerance of the *S. cerevisiae* and *C. neoformans* mutant and WT strains was compared on YPD plates supplemented with 0.8M NaCl or incubated at 37°C.

Virulence studies

This study was approved and performed in accordance with the recommendations and guidelines of the Western Sydney Local Health District Animal Ethics Committee, Department of Animal Care, Westmead Hospital. The virulence of the strains in 7-week-old female BALB/c mice (from the Animal Resource Centre, Floreat Park, Western Australia) was tested as previously described [24].

Survival: 10 mice/group were inoculated intranasally with either the WT, *arg1*Δ or the *arg1*Δ + *ARG1* strain (5 x 10^5 cells/20 µL PBS), observed daily for signs of infection over a 60-day period, and sacrificed at predetermined clinical endpoints.

Organ burden: 3 mice/group were inoculated intranasally with either the WT or the *arg1*Δ strain, and lung and brain were collected at 3, 7 and 14 days post infection to assess fungal load and histopathology.

Histopathology: Lungs were removed and fixed in 4% formalin. Sections (5 µm) were cut with a microtome and stained with Periodic Acid–Schiff (PAS) stain to identify infecting *C. neoformans* cells. Images were obtained as various magnifications using an Olympus BX43 light microscope fitted with an Olympus DP21 digital camera.

Phagocytosis assay

Fungal cells were grown overnight in YPD broth, washed with water, and heat-killed by incubating at 56°C for 30 min to prevent replication. Cells were then labelled with 0.5 mg/mL FITC (Sigma) in PBS for 30 min. Excess stain was removed by washing 4 times with PBS and the final cell pellet was resuspended in PBS. FITC-labeled fungal cells were opsonized for 30 min by incubation with 10% human serum in PBS (10^6 cells/100 µL), pelleted, and then resuspended in RPMI 1640-10% FBS medium.

Peripheral blood mononuclear cells (PBMCs) were isolated from ~25 mL human blood using Ficoll-Paque PLUS (GE Healthcare) following the manufacturer's instructions. The PBMC layer was extracted and resuspended in RPMI/10% FBS. PBMCs (4 x 10^6) were mixed with cryptococci (4 x 10^6) in 1:1 ratio in 100 µL of RPMI 1640-10% FBS medium, and co-incubation was allowed for 2 h at 37°C/5% CO_2.

The co-culture was washed once with PBS, and treated with 50 µg Fc blocking agent (mouse IgG Life Technologies, Cat. No. 02-6502; prepared working solution of 100 µg/mL in 0.5% BSA PBS with 0.05% sodium azide). The monocytes in the PBMC population were labelled with anti-CD14 BV421-conjugated antibodies (BioLegend, Cat. No. 301830). The extent of phagocytosis in 50 µL of the co-culture was determined by flow cytometry (BD FACSCanto™ II).

Comparing cell-associated and secreted Plb1 protein by Western blotting

Each strain was cultured overnight in YNB + 2% glucose. The cultures were adjusted to equal cell numbers and grown for a further 18 hours. Equal cell numbers were pelleted by centrifugation and the supernatants (protein secretions) were collected and dialyzed using SnakeSkin® Dialysis Tubing with a 10K molecular weight cut-off (Thermo Fisher Scientific). The dialyzed supernatants were snap-frozen in liquid nitrogen before being lyophilized within a Christ Alpha 2-4 freeze dryer (Martin Christ, Osterode, Germany). The dried pellets were then resuspended in 125 mM imidazole buffer (pH 4.0) and precipitated with 90% trichloroacetic acid (TCA).

Total protein and RNA from the cell pellets were extracted with TRIzol® (Thermo Fisher Scientific, Cat. No. 15596026) and used to assess the level of cell-associated Plb1 protein and *PLB1* mRNA, respectively. Briefly, the fungal cell pellets were resuspended in TRizol® and homogenized in the presence of glass beads (426-600 µm, Sigma) using a bead beater (4 cycles, 30 sec beating, 1 min rest). After homogenization, RNA and protein were prepared according to the manufacturer's instructions.

Proteins in the secreted and cell-associated fractions were dissolved in NuPAGE® sample loading buffer and reducing agent (Life Technologies). They were then resolved by SDS-PAGE using NuPAGE® 4-12% bis-Tris gels (Life Technologies) at 170V for 55 min, and transferred to a PVDF membrane (Immobilon-P 0.45 µm transfer membrane, Millipore). To detect Plb1 protein the blots were incubated with an anti-Plb1 peptide

specific antibody: 1 µg/mL in Tris-buffered saline with 0.05% Tween-20 (TBST) and 2% BSA. Production of anti-CnPlb1 antibody was described in [54]. The membranes were washed four times with TBST and then incubated with donkey-anti-goat secondary antibody (Santa Cruz Biotechnology), diluted 1:5000 in TBST with 2% BSA. Chemiluminescence was detected by exposing the membrane to Amersham Hyperfilm™ ECL (GE Healthcare) and developing the film using an X-ray developer.

PLB1 gene expression

Total RNA extracted as described above was treated with DNase and used for oligo-dT-primed cDNA synthesis. The primer pairs for amplifying *PLB1* (target gene) and *ACT1* (reference gene) cDNA were prepared at a final concentration of 2 µM each. Primer sequences were for a) *PLB1*: TCATTAGCGCACCGAGTTTG (forward) and AATGGCAAGTGGTGGTAGCC (reverse) and b) *ACT1*: ATGGTATTGCCGACCGTATG (forward) and CTCTTCGCGATCCACATCTG (reverse). *PLB1* gene expression levels in each sample, relative to *ACT1*, were then determined using SYBR Green qRT-PCR (Corbett Rotor-Gene 6000). Relative quantification of *PLB1* expression was determined using the ΔΔCt method [55].

Enzymatic removal of _N_-linked glycans

Secretions containing 40 µg protein were resuspended in 25 µL 20 mM sodium phosphate buffer (pH 7.5) and treated with 2U PNGase F (New England Biolabs P0704S). A PNGase F negative control was prepared by substituting PNGase F with 2

µL 20 mM sodium phosphate buffer. Samples were incubated at 37°C for 18 hours, after which they were dried using an Eppendorf Concentrator. Samples were then subjected to SDS-PAGE and then either stained for glycoproteins according to the manufacturer's instructions (Pierce Glycoprotein Staining Kit, catalogue number 24562) or subjected to Western blotting as per the Plb1 Western blotting protocol above.

Microscopy

Sample preparation for Transmission Electron Microscopy was carried out as described in [34]. Briefly, overnight YPD cultures of *C. neoformans* were prepared for TEM using 2% glutaraldehyde pre-fixation and 2% $KMnO_4$ post-fixation. Following resuspension in 1:1 acetone:epoxy resin, cell pellets were embedded in 100% epoxy resin. 60–80 nm sections were cut using the Leica Ultracut UCT ultramicrotome (Leica Microsystems, Bannockburn, IL), stained with uranyl acetate-lead citrate and viewed with a JEM 1200EX transmission electron microscope (JEOL, USA).

Vacuole labeling with FM 4-64 was carried out as described in [20]. Briefly, cells were grown in YPD overnight, pelleted and resuspended in fresh medium (1 ml, OD_{600} ~0.5). After addition of FM 4-64 (10 µM final concentration), the cells were stained for 5 min, pelleted, resuspended in fresh YPD medium and incubated for an additional 40 min at 30°C with shaking. The tubes were stored on ice until visualization.

Statistical analysis

Statistical analysis was carried out using SPSS Statistics software (version 24). Specifically, the Kaplan Meier Log-ranked Mantel-Cox test and the Mann-Whitney U test were used to assess survival and organ burden differences, respectively, in the mice studies. One-way analysis of variance (ANOVA) followed by Tukey-Kramer multiple comparison was used to assess *PLB1* gene expression levels and phagocytosis.

Disclosure of potential conflicts of interest

The authors declare that the research was conducted in the absence of any commercial or financial relationships that could be construed as a potential conflict of interest.

Acknowledgments

We are grateful to Virginia James from the histopathology facility at The Westmead Institute for Medical Research for technical assistance.

Funding

This work was supported by a National Health and Medical Research Council of Australia (NHMRC) project grant (APP1058779_Djordjevic). CL is supported by an Australian Postgraduate Award. SL is supported by a Westmead Institute for Medical Research (WIMR) Career Development award. AS is supported by the Medical Research Council (MRC) core support to the MRC/UCL Laboratory for Molecular Cell Biology University Unit (MC_UU_1201814). JPM is supported by a Senior Research

Fellowship from the NHMRC. TCS is supported by the Sydney Medical School Foundation.

References

1. Rajasingham R, Smith RM, Park BJ, Jarvis JN, Govender NP, Chiller TM, et al. Global burden of disease of HIV-associated cryptococcal meningitis: an updated analysis. Lancet Infect Dis 2017.

2. Williamson PR. The relentless march of cryptococcal meningitis. Lancet Infect Dis 2017.

3. Williamson PR, Jarvis JN, Panackal AA, Fisher MC, Molloy SF, Loyse A, et al. Cryptococcal meningitis: epidemiology, immunology, diagnosis and therapy. Nat Rev Neurol 2017; 13:13-24.

4. Falci DR, da Rosa FB, Pasqualotto AC. Hematological toxicities associated with amphotericin B formulations. Leukemia & lymphoma 2015; 56:2889-94.

5. Abruzzo GK, Flattery AM, Gill CJ, Kong L, Smith JG, Pikounis VB, et al. Evaluation of the echinocandin antifungal MK-0991 (L-743,872): efficacies in mouse models of disseminated aspergillosis, candidiasis, and cryptococcosis. Antimicrobial agents and chemotherapy 1997; 41:2333-8.

6. Feldmesser M, Kress Y, Mednick A, Casadevall A. The effect of the echinocandin analogue caspofungin on cell wall glucan synthesis by Cryptococcus neoformans. The Journal of infectious diseases 2000; 182:1791-5.

7. Smith KD, Achan B, Hullsiek KH, McDonald TR, Okagaki LH, Alhadab AA, et al. Increased Antifungal Drug Resistance in Clinical Isolates of Cryptococcus neoformans in Uganda. Antimicrobial agents and chemotherapy 2015; 59:7197-204.

8. Pan W, Khayhan K, Hagen F, Wahyuningsih R, Chakrabarti A, Chowdhary A, et al. Resistance of Asian Cryptococcus neoformans serotype A is confined to few microsatellite genotypes. PloS one 2012; 7:e32868.

9. Kozubowski L, Lee SC, Heitman J. Signalling pathways in the pathogenesis of Cryptococcus. Cellular microbiology 2009; 11:370-80.

10. McCotter SW, Horianopoulos LC, Kronstad JW. Regulation of the fungal secretome. Current genetics 2016; 62:533-45.

11. Rodrigues ML, Djordjevic JT. Unravelling secretion in Cryptococcus neoformans: more than one way to skin a cat. Mycopathologia 2012; 173:407-18.

12. Geddes JM, Croll D, Caza M, Stoynov N, Foster LJ, Kronstad JW. Secretome profiling of Cryptococcus neoformans reveals regulation of a subset of virulence-associated proteins and potential biomarkers by protein kinase A. BMC Microbiol 2015; 15:206.

13. Waterman SR, Hacham M, Panepinto J, Hu G, Shin S, Williamson PR. Cell wall targeting of laccase of Cryptococcus neoformans during infection of mice. Infection and immunity 2007; 75:714-22.

14. Siafakas AR, Sorrell TC, Wright LC, Wilson C, Larsen M, Boadle R, et al. Cell wall-linked cryptococcal phospholipase B1 is a source of secreted enzyme and a determinant of cell wall integrity. The Journal of biological chemistry 2007; 282:37508-14.

15. Yoneda A, Doering TL. A eukaryotic capsular polysaccharide is synthesized intracellularly and secreted via exocytosis. Molecular biology of the cell 2006; 17:5131-40.

16. Rodrigues ML, Nakayasu ES, Oliveira DL, Nimrichter L, Nosanchuk JD, Almeida IC, et al. Extracellular vesicles produced by Cryptococcus neoformans contain protein components associated with virulence. Eukaryotic cell 2008; 7:58-67.

17. Reese AJ, Doering TL. Cell wall alpha-1,3-glucan is required to anchor the Cryptococcus neoformans capsule. Molecular microbiology 2003; 50:1401-9.

18. Reese AJ, Yoneda A, Breger JA, Beauvais A, Liu H, Griffith CL, et al. Loss of cell wall alpha(1-3) glucan affects Cryptococcus neoformans from ultrastructure to virulence. Molecular microbiology 2007; 63:1385-98.

19. Levitz SM. Innate recognition of fungal cell walls. PLoS pathogens 2010; 6:e1000758.

20. Lev S, Desmarini D, Li C, Chayakulkeeree M, Traven A, Sorrell TC, et al. Phospholipase C of Cryptococcus neoformans regulates homeostasis and virulence by providing inositol trisphosphate as a substrate for Arg1 kinase. Infection and immunity 2013; 81:1245-55.

21. Wilson MS, Livermore TM, Saiardi A. Inositol pyrophosphates: between signalling and metabolism. The Biochemical journal 2013; 452:369-79.

22. Shears SB. Inositol pyrophosphates: why so many phosphates? Adv Biol Regul 2015; 57:203-16.

23. Lev S, Li C, Desmarini D, Saiardi A, Fewings NL, Schibeci SD, et al. Fungal Inositol Pyrophosphate IP7 Is Crucial for Metabolic Adaptation to the Host Environment and Pathogenicity. mBio 2015; 6:e00531-15.

24. Li C, Lev S, Saiardi A, Desmarini D, Sorrell TC, Djordjevic JT. Identification of a major IP5 kinase in Cryptococcus neoformans confirms that PP-IP5/IP7, not IP6, is essential for virulence. Scientific reports 2016; 6:23927.

25. Dubois E, Messenguy F. Pleiotropic function of ArgRIIIp (Arg82p), one of the regulators of arginine metabolism in Saccharomyces cerevisiae. Role in expression of cell-type-specific genes. Molecular & general genetics : MGG 1994; 243:315-24.

26. Dubois E, Scherens B, Vierendeels F, Ho MM, Messenguy F, Shears SB. In Saccharomyces cerevisiae, the inositol polyphosphate kinase activity of Kcs1p is required for resistance to salt stress, cell wall integrity, and vacuolar morphogenesis. The Journal of biological chemistry 2002; 277:23755-63.

27. Seeds AM, Bastidas RJ, York JD. Molecular definition of a novel inositol polyphosphate metabolic pathway initiated by inositol 1,4,5-trisphosphate 3-kinase activity in Saccharomyces cerevisiae. J Biol Chem 2005; 280:27654-61.

28. Saiardi A, Nagata E, Luo HR, Sawa A, Luo X, Snowman AM, et al. Mammalian inositol polyphosphate multikinase synthesizes inositol 1,4,5-trisphosphate and an

inositol pyrophosphate. Proceedings of the National Academy of Sciences of the United States of America 2001; 98:2306-11.

29. Cox GM, McDade HC, Chen SC, Tucker SC, Gottfredsson M, Wright LC, et al. Extracellular phospholipase activity is a virulence factor for Cryptococcus neoformans. Molecular microbiology 2001; 39:166-75.

30. Turner KM, Wright LC, Sorrell TC, Djordjevic JT. N-linked glycosylation sites affect secretion of cryptococcal phospholipase B1, irrespective of glycosylphosphatidylinositol anchoring. Biochimica et biophysica acta 2006; 1760:1569-79.

31. Chayakulkeeree M, Johnston SA, Oei JB, Lev S, Williamson PR, Wilson CF, et al. SEC14 is a specific requirement for secretion of phospholipase B1 and pathogenicity of Cryptococcus neoformans. Molecular microbiology 2011; 80:1088-101.

32. Lev S, Crossett B, Cha SY, Desmarini D, Li C, Chayakulkeeree M, et al. Identification of Aph1, a phosphate-regulated, secreted, and vacuolar acid phosphatase in Cryptococcus neoformans. mBio 2014; 5:e01649-14.

33. Djordjevic JT, Del Poeta M, Sorrell TC, Turner KM, Wright LC. Secretion of cryptococcal phospholipase B1 (PLB1) is regulated by a glycosylphosphatidylinositol (GPI) anchor. The Biochemical journal 2005; 389:803-12.

34. Chayakulkeeree M, Sorrell TC, Siafakas AR, Wilson CF, Pantarat N, Gerik KJ, et al. Role and mechanism of phosphatidylinositol-specific phospholipase C in survival and virulence of Cryptococcus neoformans. Molecular microbiology 2008; 69:809-26.

35. Chen SC, Wright LC, Golding JC, Sorrell TC. Purification and characterization of secretory phospholipase B, lysophospholipase and lysophospholipase/transacylase from a virulent strain of the pathogenic fungus Cryptococcus neoformans. The Biochemical journal 2000; 347:431-9.

36. Lev S, Kaufman-Francis K, Desmarini D, Juillard PG, Li C, Stifter SA, et al. Pho4 Is Essential for Dissemination of Cryptococcus neoformans to the Host Brain by Promoting Phosphate Uptake and Growth at Alkaline pH. mSphere 2017; 2.

37. Osterholzer JJ, Milam JE, Chen GH, Toews GB, Huffnagle GB, Olszewski MA. Role of dendritic cells and alveolar macrophages in regulating early host defense against pulmonary infection with Cryptococcus neoformans. Infection and immunity 2009; 77:3749-58.

38. Feldmesser M, Kress Y, Novikoff P, Casadevall A. Cryptococcus neoformans is a facultative intracellular pathogen in murine pulmonary infection. Infection and immunity 2000; 68:4225-37.

39. Mayr GW, Windhorst S, Hillemeier K. Antiproliferative plant and synthetic polyphenolics are specific inhibitors of vertebrate inositol-1,4,5-trisphosphate 3-kinases and inositol polyphosphate multikinase. The Journal of biological chemistry 2005; 280:13229-40.

40. Voglmaier SM, Bembenek ME, Kaplin AI, Dorman G, Olszewski JD, Prestwich GD, et al. Purified inositol hexakisphosphate kinase is an ATP synthase: diphosphoinositol pentakisphosphate as a high-energy phosphate donor. Proceedings of the National Academy of Sciences of the United States of America 1996; 93:4305-10.

41. Saiardi A, Erdjument-Bromage H, Snowman AM, Tempst P, Snyder SH. Synthesis of diphosphoinositol pentakisphosphate by a newly identified family of higher inositol polyphosphate kinases. Curr Biol 1999; 9:1323-6.

42. Szijgyarto Z, Garedew A, Azevedo C, Saiardi A. Influence of inositol pyrophosphates on cellular energy dynamics. Science 2011; 334:802-5.

43. Cross CE, Bancroft GJ. Ingestion of acapsular Cryptococcus neoformans occurs via mannose and beta-glucan receptors, resulting in cytokine production and increased phagocytosis of the encapsulated form. Infection and immunity 1995; 63:2604-11.

44. Popolo L, Gilardelli D, Bonfante P, Vai M. Increase in chitin as an essential response to defects in assembly of cell wall polymers in the ggp1delta mutant of Saccharomyces cerevisiae. Journal of bacteriology 1997; 179:463-9.

45. Terashima H, Yabuki N, Arisawa M, Hamada K, Kitada K. Up-regulation of genes encoding glycosylphosphatidylinositol (GPI)-attached proteins in response to cell wall damage caused by disruption of FKS1 in Saccharomyces cerevisiae. Molecular & general genetics : MGG 2000; 264:64-74.

46. Lagorce A, Le Berre-Anton V, Aguilar-Uscanga B, Martin-Yken H, Dagkessamanskaia A, Francois J. Involvement of GFA1, which encodes glutamine-fructose-6-phosphate amidotransferase, in the activation of the chitin synthesis pathway in response to cell-wall defects in Saccharomyces cerevisiae. European journal of biochemistry / FEBS 2002; 269:1697-707.

47. Lemmon MA, Ferguson KM, O'Brien R, Sigler PB, Schlessinger J. Specific and high-affinity binding of inositol phosphates to an isolated pleckstrin homology domain. Proc Natl Acad Sci U S A 1995; 92:10472-6.

48. Takeuchi H, Kanematsu T, Misumi Y, Sakane F, Konishi H, Kikkawa U, et al. Distinct specificity in the binding of inositol phosphates by pleckstrin homology domains of pleckstrin, RAC-protein kinase, diacylglycerol kinase and a new 130 kDa protein. Biochim Biophys Acta 1997; 1359:275-85.

49. Millard CJ, Watson PJ, Celardo I, Gordiyenko Y, Cowley SM, Robinson CV, et al. Class I HDACs share a common mechanism of regulation by inositol phosphates. Molecular cell 2013; 51:57-67.

50. Watson PJ, Fairall L, Santos GM, Schwabe JW. Structure of HDAC3 bound to co-repressor and inositol tetraphosphate. Nature 2012; 481:335-40.

51. Fukuda M, Kojima T, Kabayama H, Mikoshiba K. Mutation of the pleckstrin homology domain of Bruton's tyrosine kinase in immunodeficiency impaired inositol 1,3,4,5-tetrakisphosphate binding capacity. J Biol Chem 1996; 271:30303-6.

52. Komander D, Fairservice A, Deak M, Kular GS, Prescott AR, Peter Downes C, et al. Structural insights into the regulation of PDK1 by phosphoinositides and inositol phosphates. EMBO J 2004; 23:3918-28.

53. Losito O, Szijgyarto Z, Resnick AC, Saiardi A. Inositol pyrophosphates and their unique metabolic complexity: analysis by gel electrophoresis. PloS one 2009; 4:e5580.

54. Siafakas AR, Wright LC, Sorrell TC, Djordjevic JT. Lipid rafts in Cryptococcus neoformans concentrate the virulence determinants phospholipase B1 and Cu/Zn superoxide dismutase. Eukaryotic cell 2006; 5:488-98.

55. Livak KJ, Schmittgen TD. Analysis of relative gene expression data using real-time quantitative PCR and the 2(-Delta Delta C(T)) Method. Methods 2001; 25:402-8.

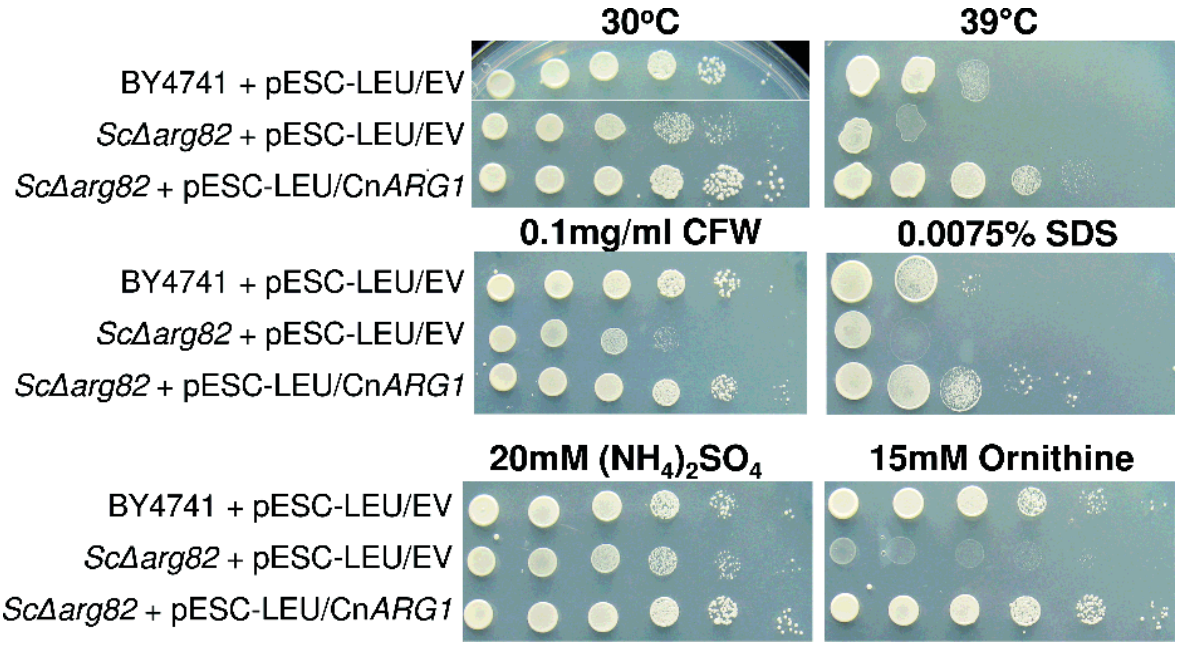

Figure 1. Arg1 from *C. neoformans* restores defective phenotypes in the *S. cerevisiae arg82*Δ mutant. *ARG1* cDNA was cloned into the pESC-LEU vector, which was then used to transform the *S. cerevisiae arg82*Δ mutant. Cells containing cloned *ARG1* or empty vector were spotted onto plates containing the various media, as indicated, from 10^6 cells per drop to 10 cells per drop. Plates were incubated at either 30°C or 39°C.

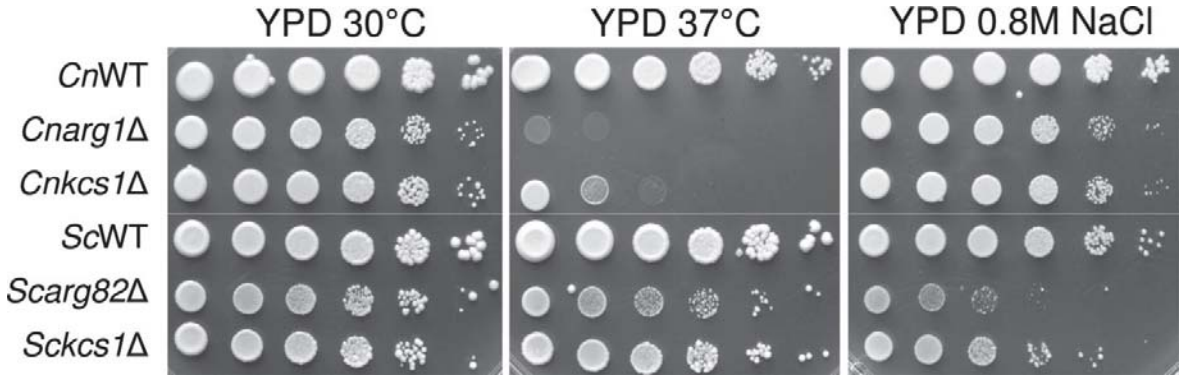

Figure 2. Arg1 and Arg82 differentially contribute to stress adaptation of *C. neoformans* and *S. cerevisiae*. WT and the indicated mutant strains were spotted onto plates containing the various media, as indicated, from 10^6 cells per drop to 10 cells per drop, and incubated for 2-4 days.

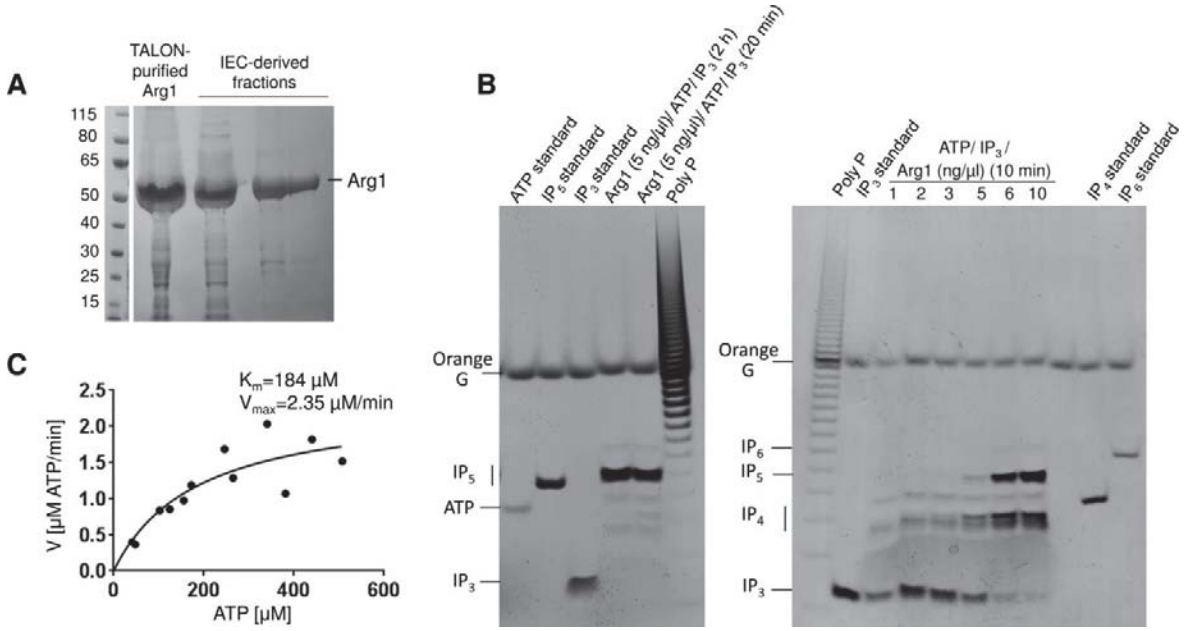

Figure 3. Purified Arg1 specifically phosphorylates IP_3 to produce IP_4 and IP_5. (**A**) Recombinant Arg1 (49 kDa, including the His_6 tag) was purified by TALON cobalt affinity chromatography followed by ion exchange chromatography (IEC). (**B**) Purified

Arg1 (1-10 ng/µl reaction, as indicated) was incubated with ATP and IP_3 and the reaction products analyzed by polyacrylamide gel electrophoresis and Toluidine Blue staining. Bands representing different IP species and ATP are indicated. (**C**) Kinetics of Arg1 activity. For these assays, purified Arg1 (20 ng) was incubated with ATP (50-500 µM) and 200 µM of IP_3 in 10 µL reactions at room temperature for 0-30 min. The consumption of ATP was monitored using bioluminescence. The assay was performed twice, each time in triplicate. V: reaction velocity.

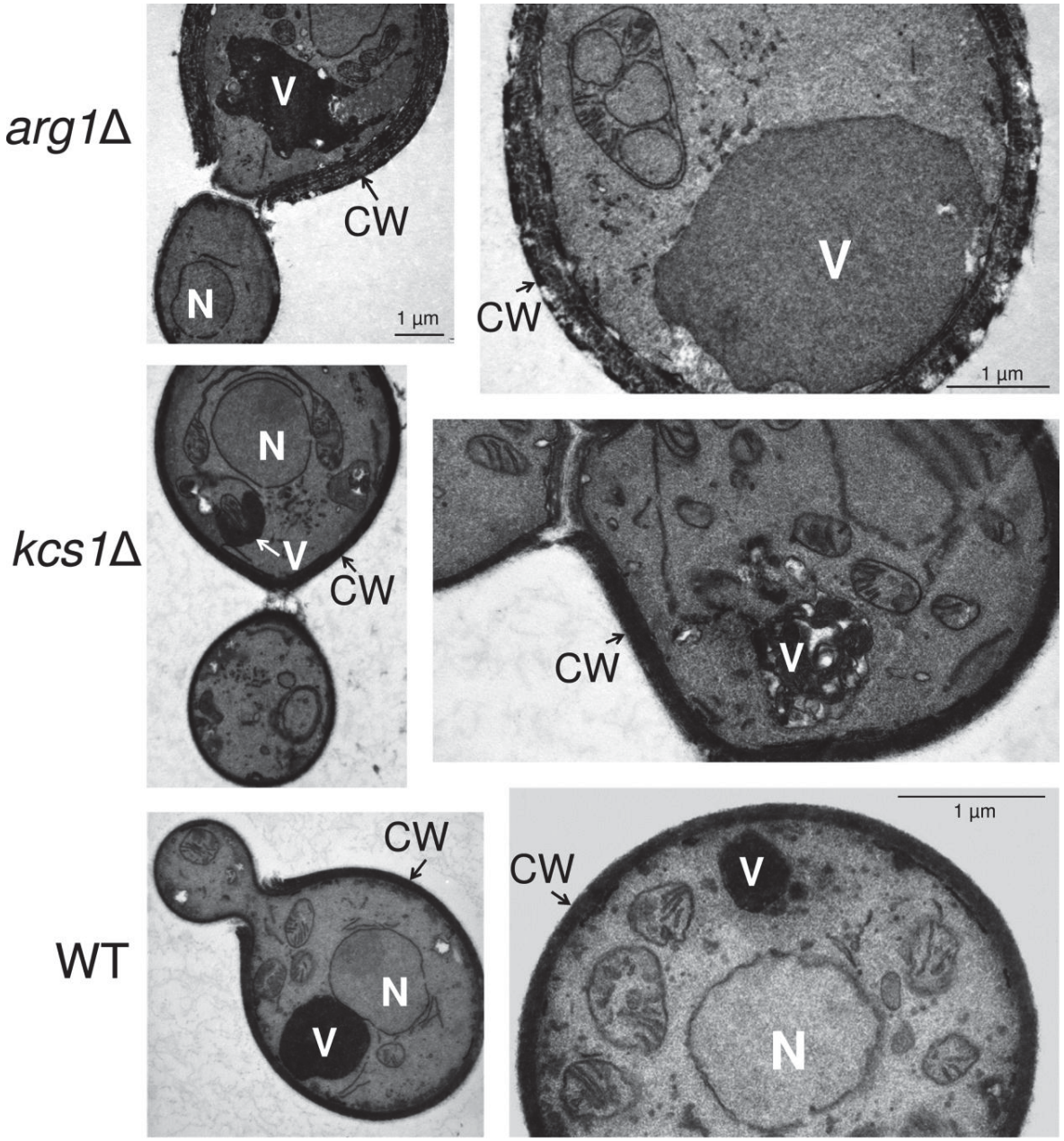

Figure 4. Comparative phenotypic testing of *arg1*Δ and *kcs1*Δ. WT, mutant and reconstituted strains were spotted onto plates containing the various media as

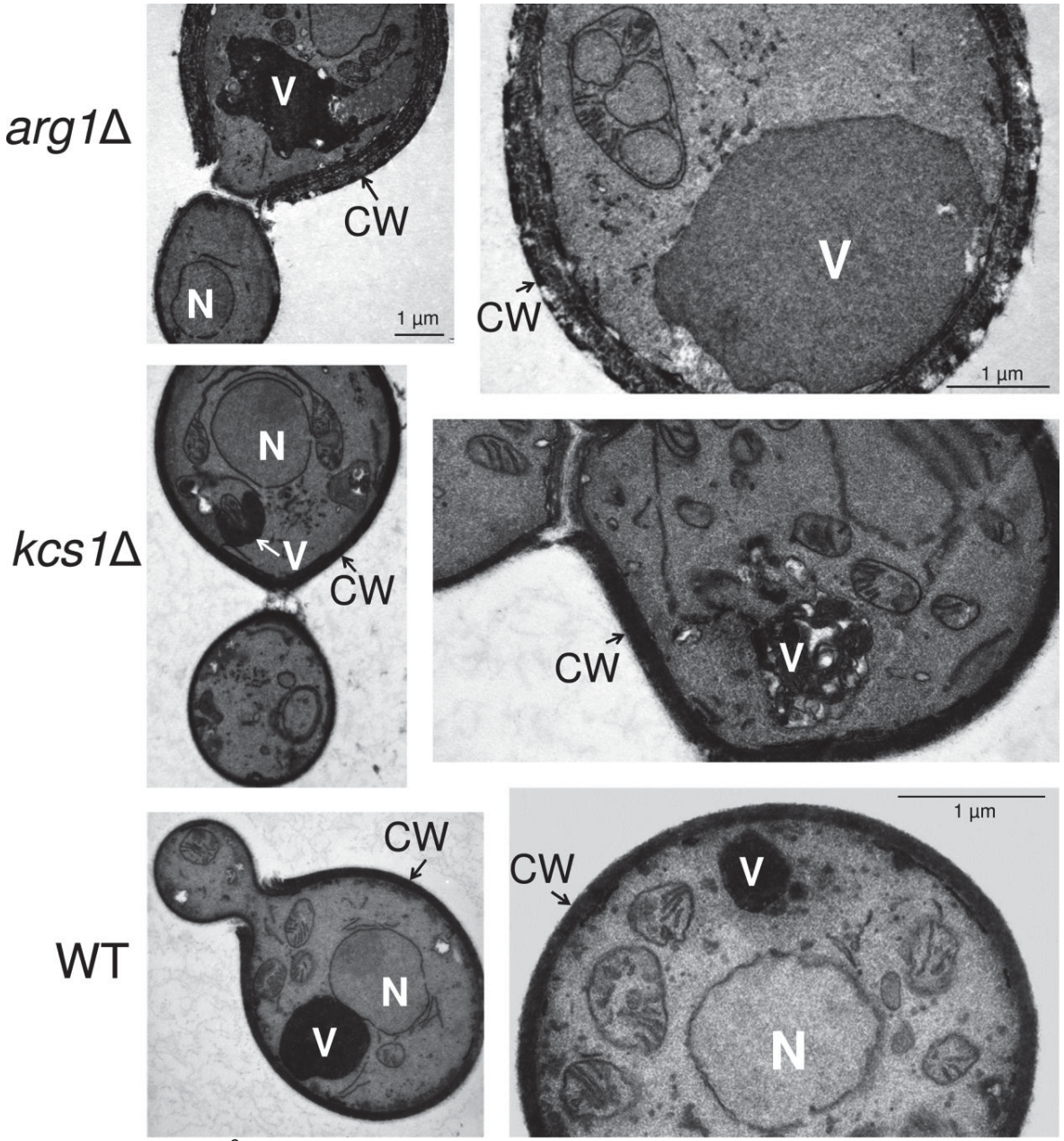

indicated, from 10^6 cells per drop to 10 cells per drop, and incubated for 2-4 days.

Figure 5. Transmission electron microscopy (TEM) demonstrating that *arg1*Δ cell walls are thicker than, and structurally different to, those of WT and *kcs1*Δ, and that *arg1*Δ cells have larger vacuoles. N: nucleus; CW: cell wall; V: vacuole.

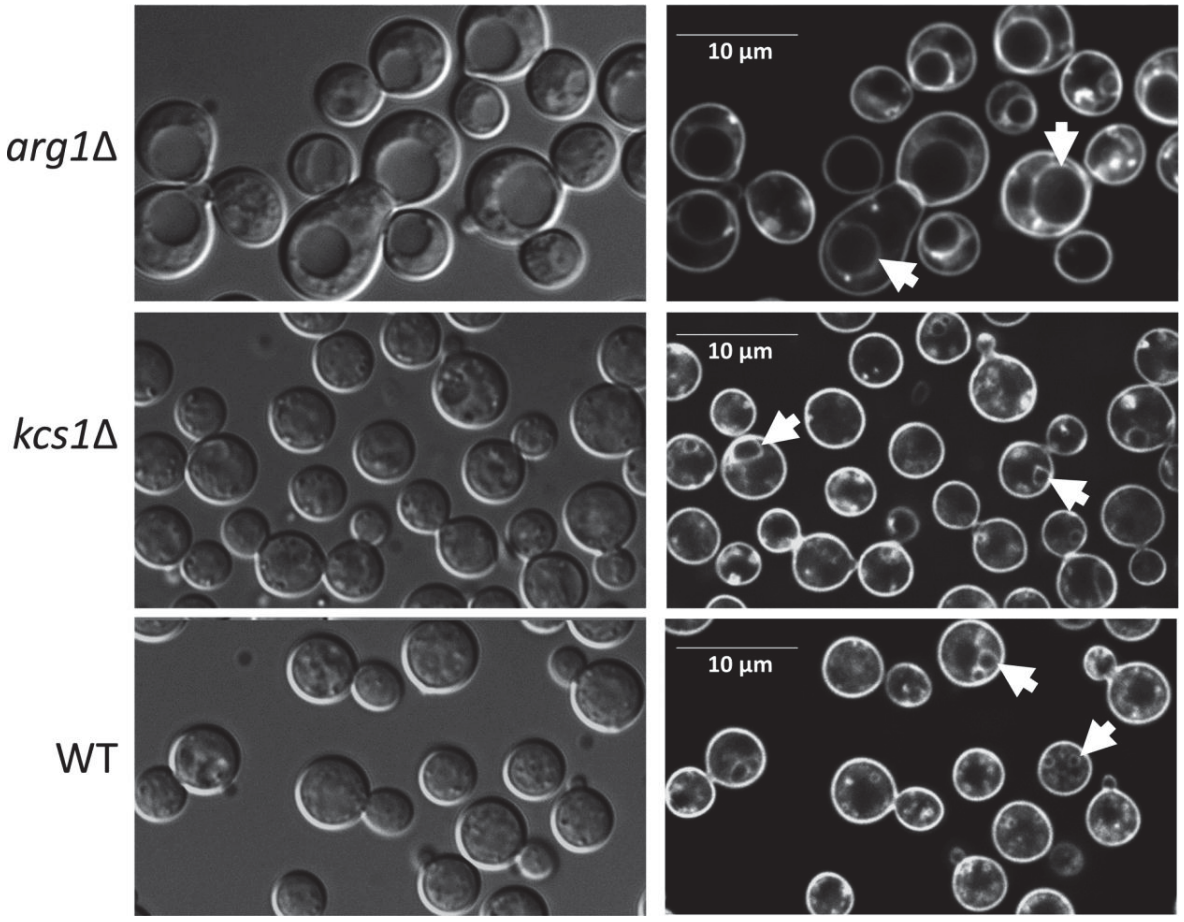

Figure 6. *arg1*Δ cells, but not *kcs1*Δ cells, are enlarged and produce bigger vacuoles. Cells were allowed to endocytose the lipophilic dye, FM 4-64, for 40 min to label vacuoles (indicated by arrows in panels on the right). Differential interference contrast images are shown on the left.

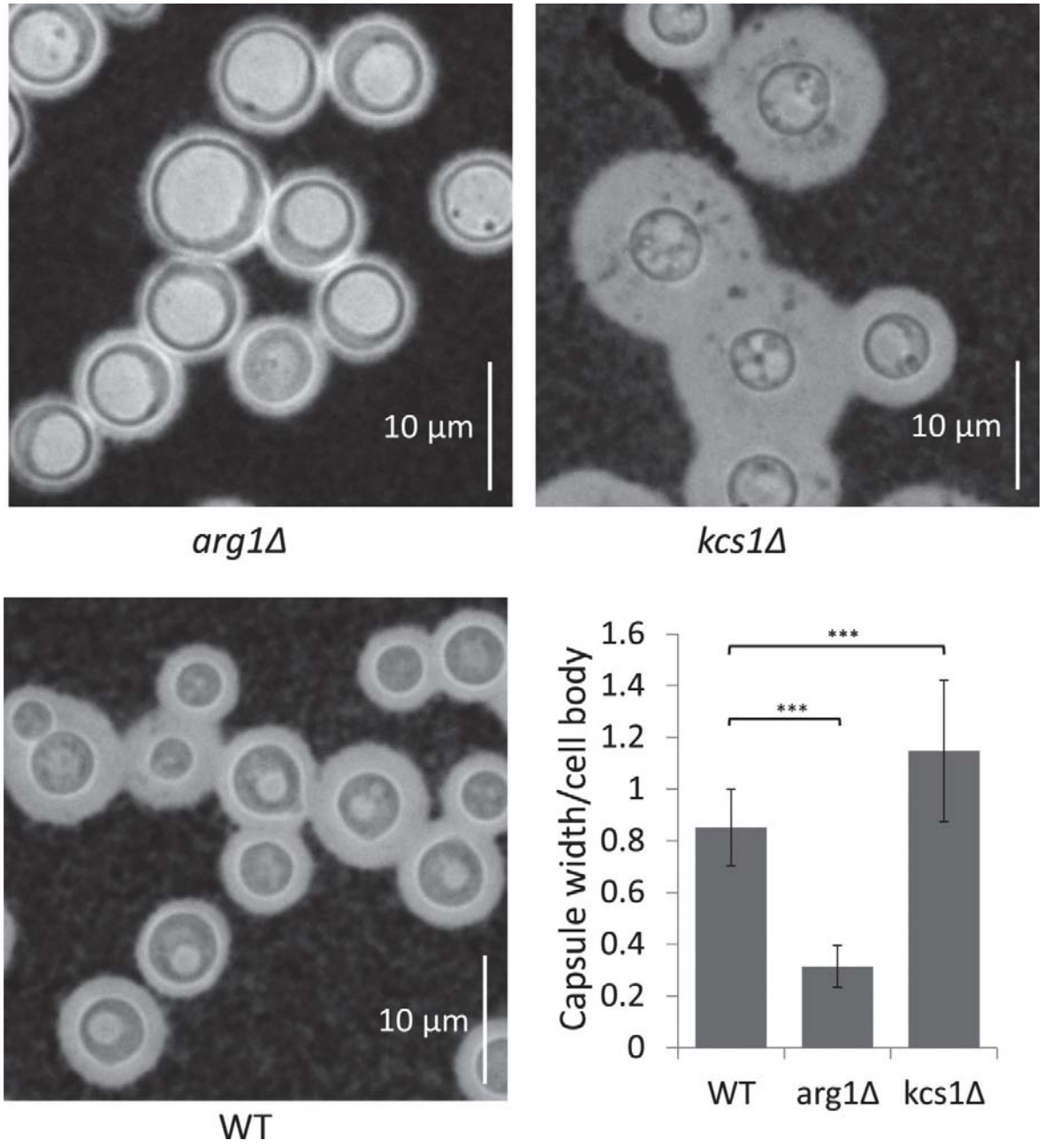

Figure 7. *arg1*Δ and *kcs1*Δ capsule size is reduced and increased, respectively, relative to WT. Cells were grown in minimal medium (broth) overnight. Capsules were visualized with India Ink stain under a light microscope at 100X magnification. The graph represents the mean ratio of capsule width to cell body diameter in each strain ±

standard deviation (n= 51 cells). ***, P<0.001 using a Tukey-Kramer multiple comparison test.

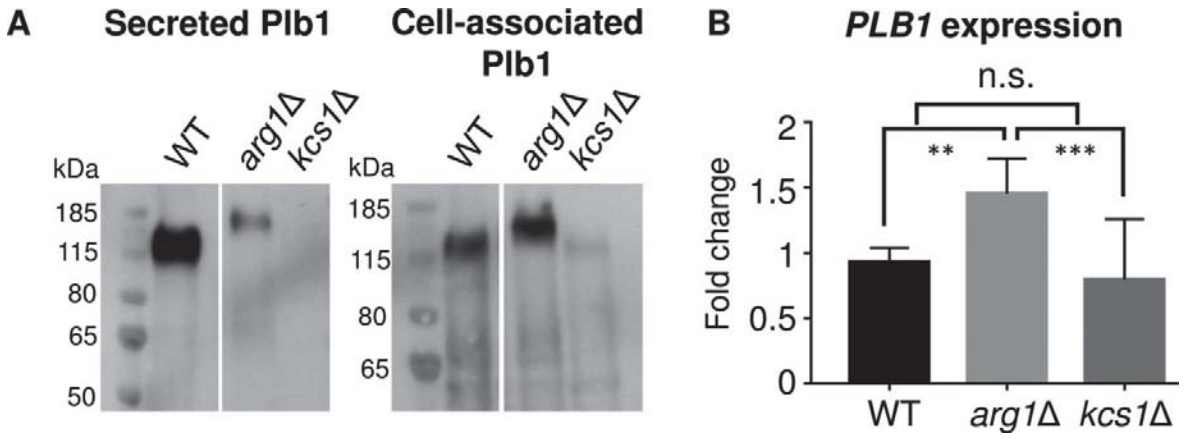

Figure 8. Blocked secretion of Plb1 in *arg1*Δ coincides with an increase in Plb1 molecular weight as assessed by Western blotting. (**A**) Plb1 in secretions and cell lysates was resolved by SDS-PAGE and detected using anti-Plb1 antibody. (**B**) *PLB1* gene expression was quantified by qPCR. The results are the average of three biological replicates ± SD. **, P < 0.01; ***, P < 0.001; n.s, not significant.

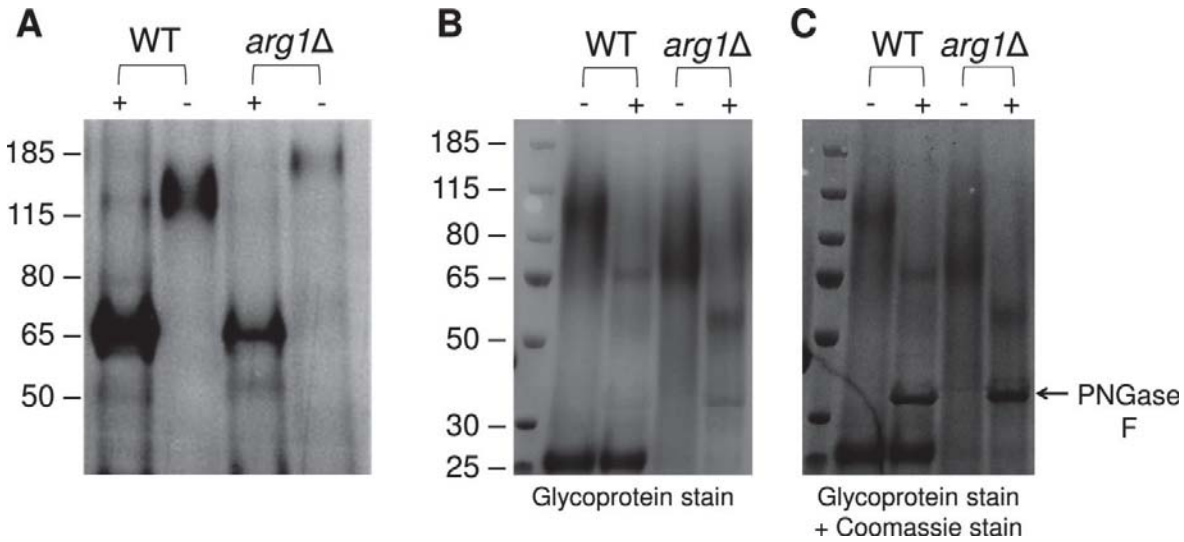

Figure 9. *N*-linked mannosylation of Plb1 and secretome composition are altered in *arg1*Δ. Cryptococcal secretions, each containing 40 μg of protein, were collected from WT and *arg1*Δ, treated with PNGase F (+), resolved by SDS-PAGE and subjected to either (**A**) anti-Plb1 Western blotting, (**B**) glycoprotein staining or (**C**) glycoprotein staining followed by Commassie staining. In (C), the arrow indicates the position of the PNGase F enzyme.

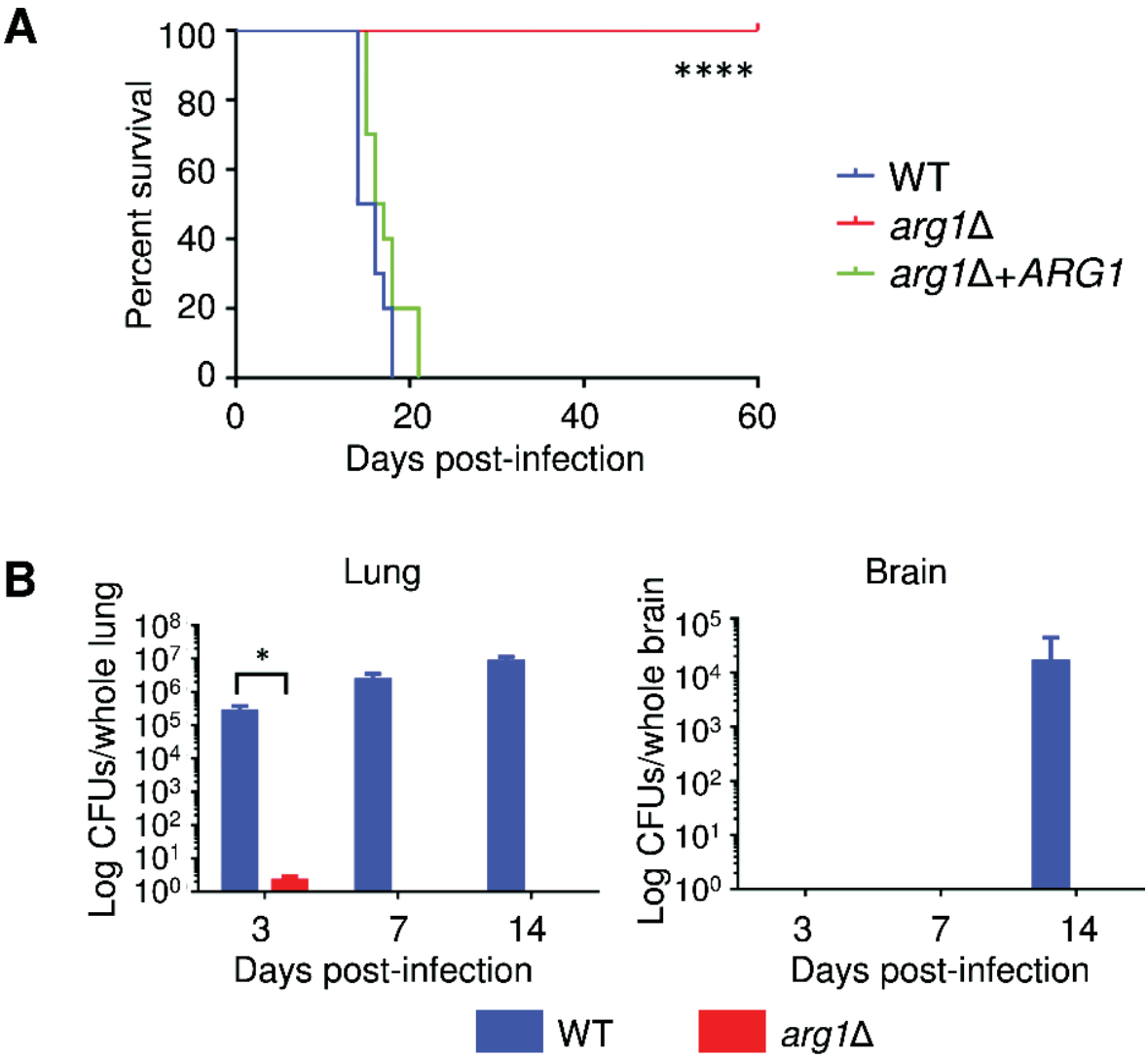

Figure 10. Arg1 is essential for lung colonization and dissemination in a murine inhalation model of cryptococcosis. (**A**) *arg1*Δ is avirulent compared to WT and *arg1*Δ + *ARG1*. Mice (n=10 per strain) were inoculated intranasally with 5 x 10^5 cells/20 µL and monitored daily. Difference in survival between WT/*arg1*Δ + *ARG1*-infected mice and *arg1*Δ-infected mice is statistically significant (**** P < 0.0001). (**B**) and (**C**) *arg1*Δ infection is rapidly cleared from mouse lung between 3 and 7 days post-infection. Mice (n=3 per strain) were inoculated intranasally with 5 x 10^5 cells/20 µL and sacrificed on the days indicated. Lung and brain were harvested for quantitative culture (CFUs) (**B**) or histopathological analysis for lung only by Periodic acid–Schiff (PAS) staining (**C**). In (**B**), the difference in lung CFUs for WT and *arg1*Δ-infected mice at day 3 is statistically significant (* P < 0.05). In (**C**), lung histopathology is shown at 3 days post-infection (PAS stain, 40x magnification). In WT-infected lung tissue, arrows indicate cryptococcomas where capsular material is represented by white halos surrounding the cell bodies (stained magenta). In *arg1*Δ-infected tissue, arrows indicate single acapsular cryptococcal cells.

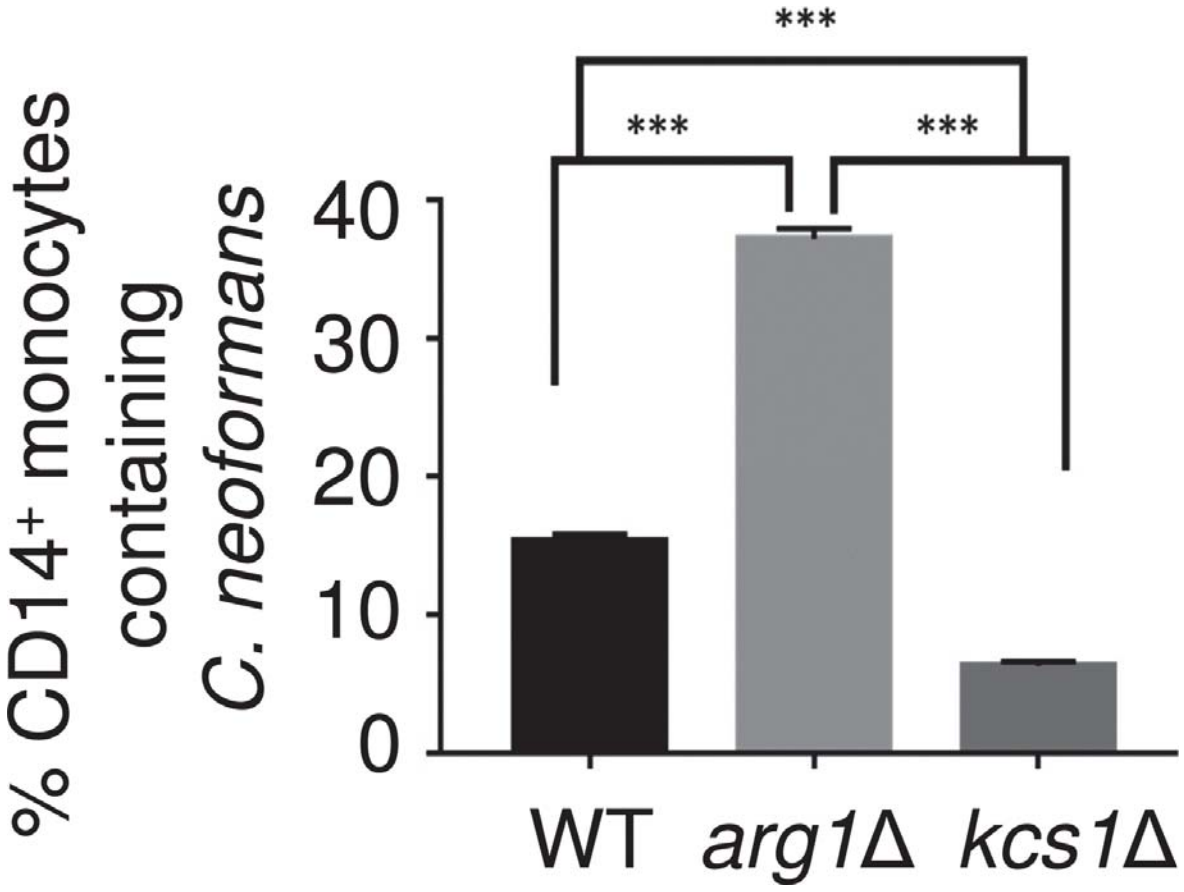

Figure 11. *arg1*Δ is more readily phagocytosed by human PBMCs. Results are expressed as the mean % of $CD14^+$ monocytes containing FITC-labelled *C. neoformans* ± SD (n=3). Statistical significance is indicated as follows: *** $P < 0.001$.

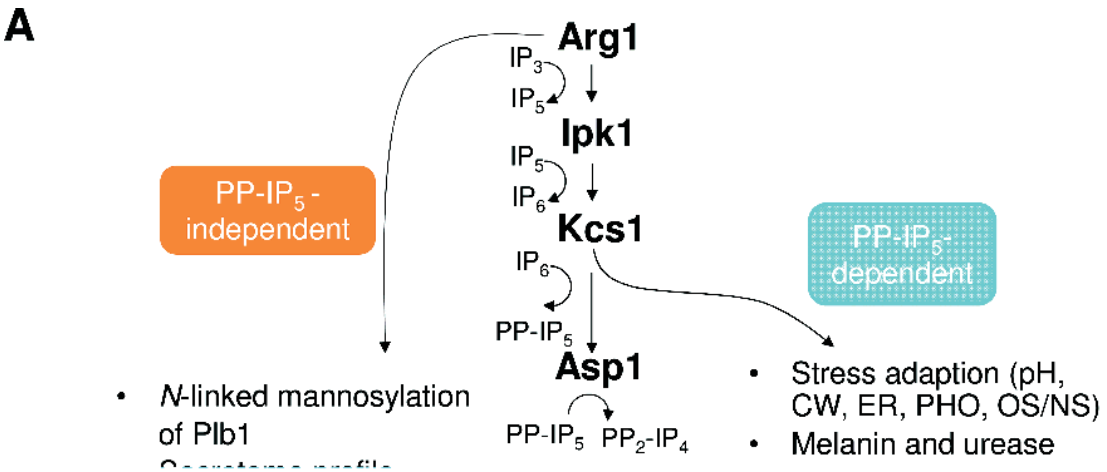

Figure 12. Summary of PP-IP_5-dependent and –independent functions of Arg1 (**A**), and the contribution of Arg1 and Kcs1 to virulence (**B**). pH – alkaline pH stress; CW – cell wall stress induced by calcofluor white, Congo red, SDS, caffeine; ER – endoplasmic reticulum stress caused by tunicamycin and DTT; PHO – phosphate deprivation; OS/NS – oxidative and nitrosative stress, respectively.

